Micromolding three-dimensional amorphous metal structures

Jeffrey A. Bardt
Department of Mechanical and Aerospace Engineering, University of Florida, Gainesville, Florida 32611

Gerald R. Bourne[a)]
Department of Materials Science and Engineering, University of Florida, Gainesville, Florida 32611

Tony L. Schmitz and John C. Ziegert
Department of Mechanical and Aerospace Engineering, University of Florida, Gainesville, Florida 32611

W. Gregory Sawyer
Department of Mechanical and Aerospace Engineering and Department of Materials Science and Engineering, University of Florida, Gainesville, Florida 32611

(Received 31 May 2006; accepted 1 September 2006)

In this article, we report a simple and inexpensive approach to micromolding of complex, three-dimensional, high aspect ratio structures (with non-line-of-sight features) out of a high-strength amorphous metal. Inexpensive sacrificial silicon molds were created using lithography and etching techniques originally developed for integrated circuit production by the microelectronics industry and later adopted for microelectromechanical (MEMS) manufacturing. Multiple silicon layers were stacked, and the metallic glass was forced into the cavities under heat and pressure in an open air environment. Following cooling, the metallic structures were released by etching the silicon away in a potassium hydroxide (KOH) bath. Process studies showed that temperature is the most significant variable governing mold-filling. Transmission electron microscopy (TEM) sections of the mold/glass interface showed successful replication of features with characteristic dimensions on the order of 10 nanometers and no discernible gap between the silicon and the metallic glass. This scalable micromolding process leverages the inexpensive and readily available aspects of silicon lithography to economically support the mass customization (low volume production) of metal microcomponents without elaborate infrastructure needs.

I. INTRODUCTION

Over the past decades, electronics technology has shown a steady trend toward miniaturization of components and circuits that has, in turn, enabled a new class of electromechanical devices known generically as microelectromechanical systems (MEMS). The application of MEMS technology to domains such as microscale sensors (chemical, fluidic, radiation, and acceleration) and power sources (batteries, photovoltaics, and energetics) has raised awareness of the potential advantages that could be realized if it were possible to miniaturize mechanical devices and systems that do not possess nearly planar geometries. However, the ability to accomplish this miniaturization is restricted by the available manufacturing technology and materials.

Interest in producing components for micro- and mesoscale mechanical systems that require materials, geometries, and/or relative tolerances that cannot be produced using conventional planar, lithography-based, surface micro-machining techniques and other MEMS fabrication technologies has led to various manufacturing alternatives. The four generic processes that are currently being investigated are material removal, material addition, casting and molding, and forming. Material removal processes include machining,[1] grinding, electrical discharge machining,[2] electrochemical machining,[3] and other microscale analogies to conventional macroscale technologies. Additive manufacturing processes create structures layer by layer, typically using electroplating followed by planarization and selective etching.[4] Casting and molding processes are routinely practiced for polymeric microscale components. Forming processes create geometry through plastic deformation, which at the microscale are generally limited to relatively simple features with

[a)]Address all correspondence to this author.
e-mail: grb@ufl.edu
DOI: 10.1557/JMR.2007.0035

low aspect ratios and are significantly impacted by inhomogeneities and anisotropies.

The durability and reusability of macroscale molds enables high-volume production of low-cost metallic or polymeric components. This process model has been extended to create microscale components of plastics, which is aided in part by the relatively low processing temperatures. The shrinkage associated with crystallization and cooling from the generally higher temperatures required for molding metal components represents a substantial technical barrier for the miniaturization of metal microcomponents. However, this limitation can be countered through the use of amorphous metals that have low glass transition temperatures and no crystallization-related shrinkage. For this study we used a widely studied bulk metallic glass of the following composition: $Zr_{41.2}Ti_{13.8}Cu_{12.5}Ni_{10}Be_{22.5}$.[5–9] This material has a glass transition temperature of approximately 350 °C[10]; above this temperature, the material is viscous and the measured viscosity is a strong function of temperature. The required cooling rate for retention of this metallic glass's amorphous structure is also low at ~10 K/s,[5,10] which is thousands of times lower than what is needed to "freeze-in" the amorphous structure for conventional metallic alloys. At our processing temperatures near 400 °C, we anticipate thermal expansion-related part shrinkages to be less than 0.5% and expect the micromolded components to have the same amorphous structure and mechanical, electrical, and thermal conductivities as their macroscale counterparts. As a family, these amorphous alloys have high yield strength, hardness, and elastic limit (thermal and electrical properties typically follow rules-of-mixture and are similar to other metallic alloys).[11,12] The material used in this study has a yield strength of 1.9 GPa and an elastic limit of approximately 2% strain; this yield strength surpasses titanium alloys with about twice the elastic limit.[10]

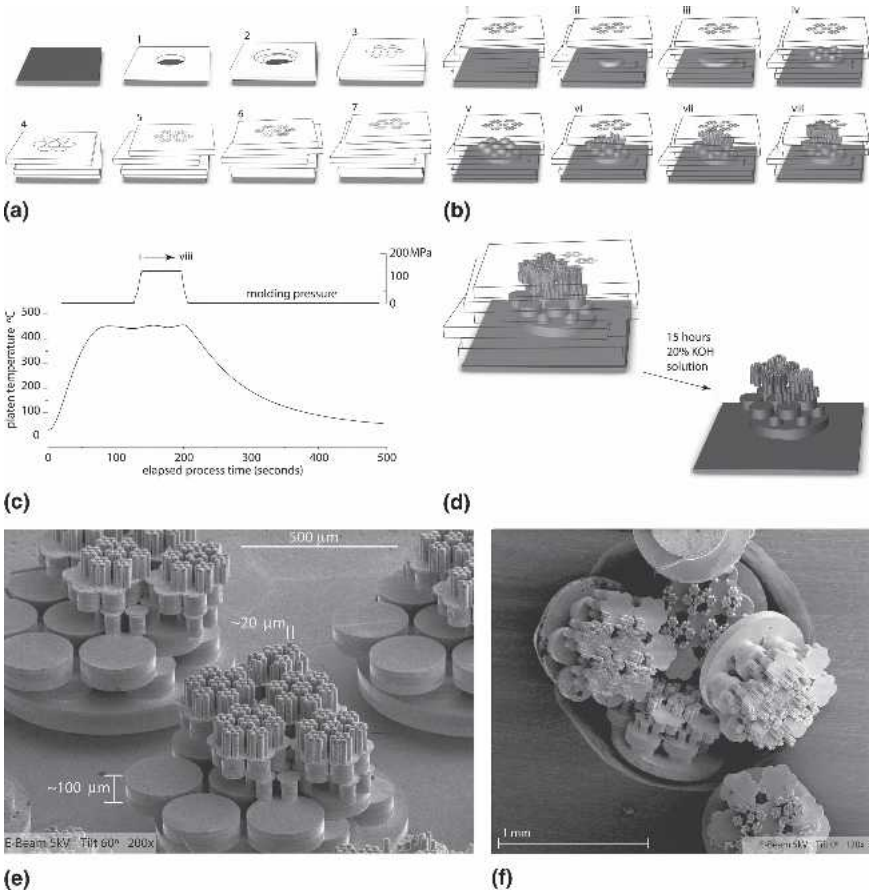

FIG. 1. Steps in the amorphous metal micromolding process: (a) After patterning by deep reactive ion etching, one or more silicon wafers are stacked to form the sacrificial mold (a seven-layer stack was used in this test; the lack of a careful alignment procedure between layers is depicted). The amorphous metal coupon is placed under the mold. (b) Once the glass transition temperature of the amorphous metal is exceeded, pressure is applied to force the reduced viscosity metal through the wafer stack. (c) The pressure and temperature profiles are displayed. (d) After cooling, the silicon-metal composite is removed from the micromolding platform. The metallic component is visible after etching. (e) SEM image of micromolded features; non-line-of-sight geometries were formed by the selected mold geometry. For this test, it is seen that the imperfect wafer alignments yielded an asymmetric product. (f) SEM image of released features after using the abrasive polishing method.

II. PROCEDURES

In this study, we constructed molds by stacking etched silicon wafers to form cavities. For these experiments, no particular care was taken to align the layers to better than a few hundred micrometers, and no bonding of the wafer mold layers was used. The cavities were then filled by forced flow of the amorphous metal. The production sequence using this approach is illustrated in Fig. 1. The individual silicon mold layers were patterned by deep reactive ion etching, which can be used to produce two-dimensional features with aspect ratios as high as 10:1. This parallel fabrication technique is well-suited to our process; for our 5 × 5 mm square mold sections, over 150 unique designs can be patterned on a single 100-mm diameter wafer. To create complex non-line-of-sight cavities, we stacked multiple silicon wafers with the desired geometries [Fig. 1(a)]. These layers were placed, together with a layer of amorphous metal, into a square pocket machined into a stainless steel block. The block had 2.5 kW electrical heating power supplied through cartridge-type heaters with integral pathways for water cooling and was attached to a load frame with force and displacement control capabilities. The layered mold and the amorphous metal were heated to the process temperature, and pressure was applied to the amorphous metal layer, forcing it into the mold cavities [Fig. 1(b)]. This was followed by rapid cooling. A typical process was completed in less than 500 s, and the molding pressures were between 100 and 200 MPa [Fig. 1(c)]. The integral part, made up of the silicon layers and the amorphous metal, was then removed from the platform, and the silicon was etched away using a heated potassium hydroxide (KOH) solution [Fig. 1(d)], leaving molded structures of amorphous metal attached to the base. We have successfully demonstrated fabrication of complex microscale parts made up of seven mold layers [Fig. 1(e)] that can be fully released by abrasively polishing the base down to the silicon mold layer prior to KOH etching [Fig. 1(f)]. This micromolding process can be used to manufacture small batches of unique metallic microcomponents in a cost-effective manner; the costs scale with the number and size of the silicon layers needed to form the mold but not the complexity of the cavities within the individual layers.

III. RESULTS AND DISCUSION

The process is able to successfully reproduce the internal cavities created by stacking the silicon layers; in Fig. 1(e) the posts on the seventh layer are 20 μm in diameter, 100 μm tall, and separated by 10 μm. Scanning electron microscopy (SEM) of the released amorphous metal structures and internal surfaces of the mold suggest that this method reproduced the internal surface topography of the silicon mold to better than a micrometer. To examine this more quantitatively, a cross section of the molded stack containing both the amorphous metal and the seven layers of etched silicon was prepared using

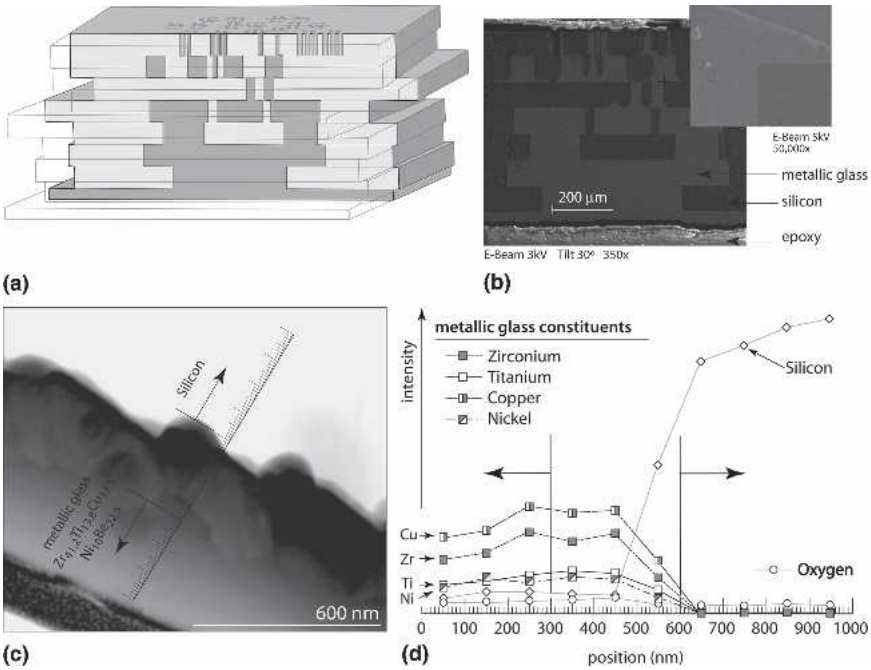

FIG. 2. Cross section of the silicon/metallic glass interface: (a) A cross section of the seven layer mold shown in Fig. 1 is depicted. (b) SEM image of filled silicon mold. The inset shows the excellent filling capabilities of the process. (c) TEM image of the metallic glass (left)/silicon (right) interface. Between the metal and silicon, a crystallized material layer approximately 180 nm thick is observed. This layer may be responsible for the absence of a gap between the silicon and metal after cooling. (d) Energy dispersive spectroscopy elemental analysis through the metallic glass/silicon interface, suggesting primarily metallic glass constituents in the integral crystallized region.

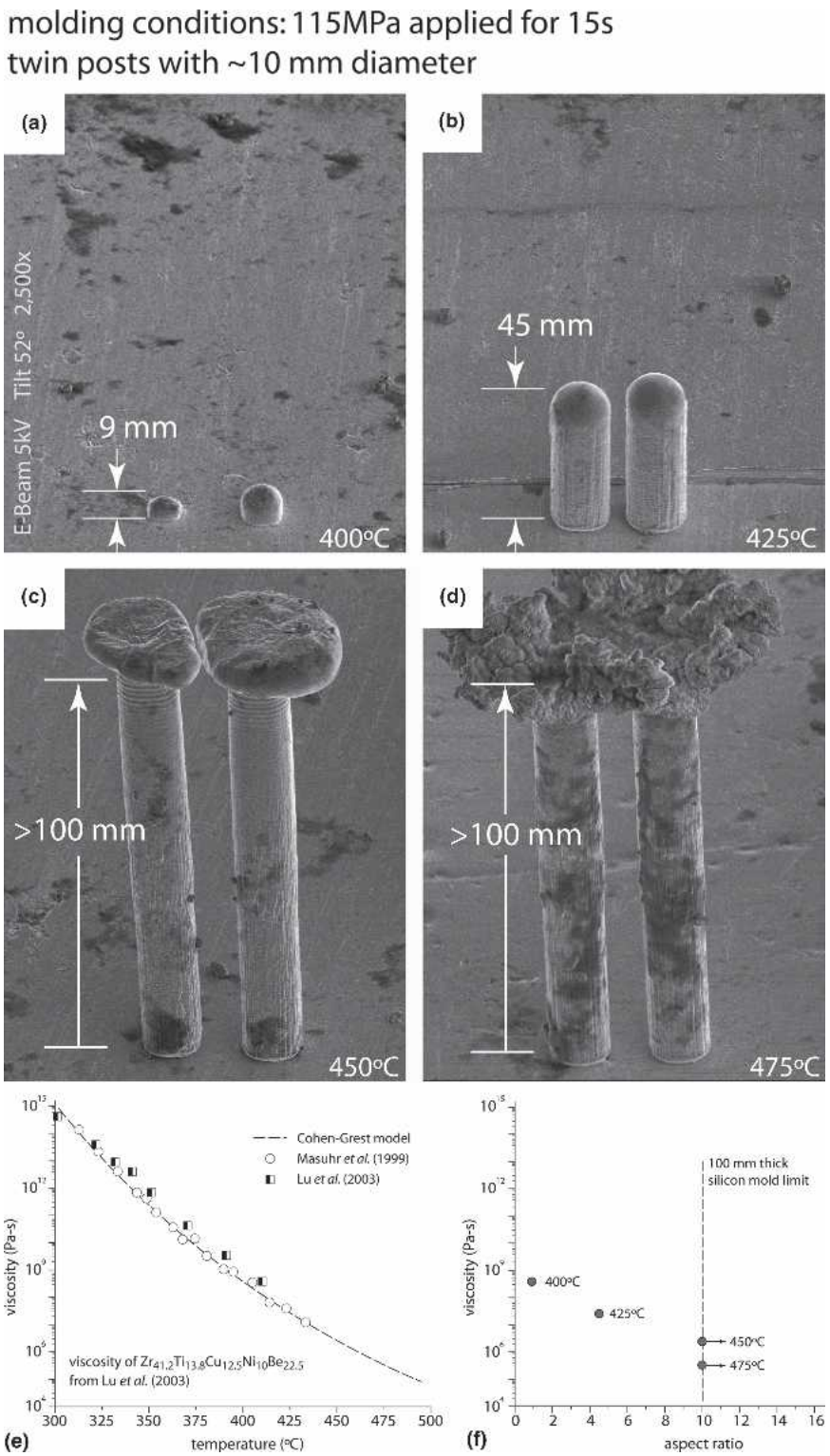

FIG. 3. Results for twin 10-μm-diameter circular posts molding study: (a) process molding temperature 400 °C, corresponding aspect ratio ~1; (b) 425 °C, aspect ratio ~4.5; (c) 450 °C, aspect ratio >10; (d) 475 °C, aspect ratio >10; (e) viscosity–temperature relationship for $Zr_{41.2}Ti_{13.8}Cu_{12.5}Ni_{10}Be_{22.5}$ over the process operating temperatures[10,13,14]; (f) increasing aspect ratios as a function of temperature limited to 10:1 by the deep reactive ion etching production of the silicon molds; higher aspect ratios for both the 450 and 475 °C conditions may be possible.

traditional metallographic techniques [Fig. 2(a)]. Examination of the section shows that the amorphous metal filled the mold without visible voids at the mold/metal interface [Fig. 2(b)]. This is surprising since the coefficient of thermal expansion of the metallic glass, 10 μm/m K, is approximately four times that of silicon, 2.6 μm/m K. For a post with a nominal diameter of 200 μm and a 400 °C temperature change, the difference in shrinkage between the silicon and the metallic glass should be on the order of 100 nm and visible in the high-resolution SEM image. A very thin slice (<200 nm) through the mold/metal interface was collected from this sample by focused-ion-beam milling. Transmission electron microscopy (TEM) analysis of the slice revealed that a layer of crystallized material approximately 180 nm thick existed at the continuous interface [Fig. 2(c)]. The lack of observable separation at the interface due to shrinkage was further supported by the cross section behavior; the silicon and metal interface remained intact during the slice lift-out procedure. One hypothesis is that the metallic atoms may chemically react with the silicon and oxygen in the mold cavity to create an integral crystallized layer. Such a reaction process may provide the necessary driving force to follow the intricate surfaces of the mold, and surface reactivity may be an important criterion for net shape fabrication of micromolded components. Energy dispersive spectroscopy (EDS) analysis through this region [Fig. 2(d)] suggests that its constituents are primarily from the amorphous metal. An added benefit of the stacked wafer approach is that the flatness of the silicon wafers and the molding pressure appear to completely arrest unintentional flow of amorphous metal between the layers; this ability to mold complex parts without flash negates the need for secondary finishing operations (assuming they were readily available).

Of the variables thought to be critical in the molding process–temperature, pressure, and time—temperature is the most important; a 15 °C increase in mold temperature reduces the viscosity by nearly an order of magnitude. In one particular study, a temperature increase from 400 to 475 °C [Figs. 3(a)–3(d)] reduced the viscosity by ~1000× [Fig. 3(e)] and increased the achievable aspect ratio from approximately unity to greater than 10:1 [Fig. 3(f)] for twin 10-μm-diameter circular posts. Although still a very viscous material at these processing temperatures, pressure-driven flow in microchannels is not entirely unexpected. Assuming fully developed flow within circular pipes, the conditions shown in Fig. 3 suggest an average velocity of the amorphous metal at 450 °C on the order of 2 μm/s [$\overline{V} = R^2/(8\ \mu)\cdot\Delta P/\Delta L$): $R = 5$ μm, $\mu = 2 \times 10^6$ Pas, $\Delta P/\Delta L = 115 \times 10^6$ Pa/100 μm].

IV. CONCLUSIONS

Given this micromolding capability and the unique properties of amorphous metals, we envision fabrication opportunities for new microcomponents with complex geometries in disciplines ranging from thermal management to the biomedical sciences. Example applications could include high-Q (lightly damped) micro-resonators for the telecom industry, high surface area structures, microwave waveguides and connectors suitable for higher frequency operation, multi-degree of freedom flexure-based micromechanisms, microsurgical tools and devices, microscale motors and transmission components, microfluidic arrays, and free-form reflective microoptics. In the end, we anticipate this new ability to create three-dimensional, metallic structures in a cost-effective manner will enable new design innovations, similar to the paradigm shift realized through the application of planar silicon fabrication technology to MEMS production.

REFERENCES

1. J. Bustillo, R. Howe, and R. Muller: Surface micromachining for microelectromechanical systems. *Proc. IEEE* **86,** 1552 (1998).
2. D. Reynaerts, P. Heeren, and H. Van Brussel: Microstructuring of silicon by electro-discharge machining (edm). 2. Applications. *Sens. Actuators, A Phys.* **61,** 379 (1997).
3. B. Bhattacharyya, J. Munda, and M. Malapati: Advancement in electrochemical micro-machining. *Int. J. Machine Tools Manufact.* **44,** 1577 (2004).
4. S. Michaelis, H. Timme, M. Wycisk, and J. Binder: Acceleration threshold switches from an additive electroplating mems process. *Sens. Actuators, A Phys.* **85,** 418 (2000).
5. A. Peker and W. Johnson: A highly processable metallic-glass-$Zr_{41.2}Ti_{13.8}Cu_{12.5}Ni_{10.0}Be_{22.5}$. *Appl. Phys. Lett.* **63,** 2342 (1993).
6. Y. Kim, R. Busch, W. Johnson, A. Rulison, and W. Rhim: Metallic-glass formation in highly undercooled $Zr_{41.2}Ti_{13.8}Cu_{12.5}Ni_{10.0}Be_{22.5}$ during containerless electrostatic levitation processing. *Appl. Phys. Lett.* **65,** 2136 (1994).
7. R. Busch, Y. Kim, and W. Johnson: Thermodynamics and kinetics of the undercooled liquid and the glass-transition of the $Zr_{41.2}Ti_{13.8}Cu_{12.5}Ni_{10.0}Be_{22.5}$ alloy. *J. Appl. Phys.* **77,** 4039 (1995).
8. X. Lin and W. Johnson: Formation of Ti–Zr–Cu–Ni bulk metallic glasses. *J. Appl. Phys.* **78,** 6514 (1995).
9. K. Ohsaka, S. Chung, and W. Rhim: Specific volumes of the $Zr_{41.2}Ti_{13.8}Cu_{12.5}Ni_{10.0}Be_{22.5}$ alloy in the liquid, glass, and crystalline states. *Appl. Phys. Lett.* **70,** 726 (1997).
10. J. Lu, G. Ravichandran, and W. Johnson: Deformation behavior of the $Zr_{41.2}Ti_{13.8}Cu_{12.5}Ni_{10.0}Be_{22.5}$ bulk metallic glass over a wide range of strain-rates and temperatures. *Acta Mater.* **51,** 3429 (2003).
11. W. Klement, R. Willens, and P. Duwez: Non-crystalline structure in solidified gold-silicon alloys. *Nature* **187,** 869 (1960).
12. W. Johnson: Bulk metallic glasses—A new engineering material. *Curr. Opin. Solid State Mater. Sci.* **1,** 383 (1996).
13. A. Masuhr, R. Busch, and W. Johnson: Thermodynamics and kinetics of the $Zr_{41.2}Ti_{13.8}Cu_{10.0}Ni_{12.5}Be_{22.5}$ bulk metallic glass forming liquid: Glass formation from a strong. *J. Non-Cryst. Solids* **252,** 566 (1999).
14. A. Masuhr, T. Waniuk, R. Busch, and W. Johnson: Time scales for viscous flow, atomic transport, and crystallization in the liquid and supercooled liquid states of $Zr_{41.2}Ti_{13.8}Cu_{12.5}Ni_{10.0}Be_{22.5}$. *Phys. Rev. Lett.* **82,** 2290 (1999).